Metals and Materials International (2023) 29:1775–1785
https://doi.org/10.1007/s12540-022-01320-7

Ultrafast Sinter Bonding Between Cu Finishes Under Moderate Compression Using In Situ Derived Ag Formed via Low-Temperature Decomposition of Ag_2O in the Bonding Paste

Yun-Ju Lee[1] · **Jong-Hyun Lee**[1]

Received: 5 August 2022 / Accepted: 23 September 2022 / Published online: 4 November 2022
© The Author(s) under exclusive licence to The Korean Institute of Metals and Materials 2022

Abstract

To accomplish rapid chip attachment and produce a bondline between Cu finishes that provides both high-temperature thermo-mechanical reliability and superior thermal conductance, compression-assisted sinter bonding at 300 ℃ was performed in air through the in situ formation of active Ag atoms by the decomposition of 200 nm Ag_2O during a redox reaction in the bonding paste. The remarkable sinterability of the generated Ag atoms and the effect of the reducing agent, which was added to the paste to remove the oxide layer on the Cu finish, induced extremely rapid sinter bonding between Cu finishes. Accordingly, the bonding under compression of 2 and 5 MPa resulted in a sufficient shear strength exceeding 27.0 MPa with a dense bondline microstructure even after a significantly short bonding time of 30 s. Transmission electron microscopy revealed that the bonding between the bondline and Cu finish was accomplished through the overlapping of Ag and Cu lattices by inter-diffusion of Ag and Cu atoms without the formation of any compound. Therefore, high-speed chip attachment was successfully achieved even for low-cost Cu finishes.

Keywords Sinter bonding · Chip attachment · Decomposition · Redox reaction · Shear strength

1 Introduction

Some of the current common soldering processes used for the production of joints that are thermo-mechanically stable at high temperatures (200–300 ℃) and bondlines that have remarkable thermal conductivity are being replaced by sinter-bonding techniques using Ag particles, especially for those involving the attachment of wide-bandgap semiconductor chips (SiC and GaN) during the fabrication of power modules for electronic vehicles, aircrafts, space exploration, and underground well logging [1–10]. However, three limitation are still to be overcome: bonding requires more time than soldering due to the involvement of solid-state sintering, the nano-sized particles used to enhance the sinterability are expensive and tend to undergo severe aggregation, and Ag particles are generally compatible with bonding on an Ag finish, which induces an additional fabrication cost when using an Ag coating on a Cu finish [5].

As typical results of high-speed sinter bonding, Ide et al. reported excellent shear strength approaching 40 MPa in a joint after 5 MPa compression bonding for 5 min at 300 ℃ using ~ 11 nm Ag nanoparticles [9]. Yan et al. performed sinter bonding of an Ag-plated Cu disc using a paste containing polyvinylpyrrolidone-absorbed Ag nanoparticles and attained a strength exceeding 20 MPa with 5 min of bonding at 200 ℃ after pre-drying at 80 ℃ [10].

To devise a sinter-bonding technique that can bond competitive surface finishes with high productivity in an air atmosphere without using nanoparticles, an attempt was made to dramatically increase the attachment speed of a Cu-finished chip under an appropriate compression pressure using submicrometer Ag_2O particles. Since Ag_2O decomposes at approximately 400 ℃, adding a solvent when preparing the bonding paste can induce the generation of Ag nanoparticles through decomposition at significantly low temperatures: the addition of myristyl alcohol [11], polyethylene glycol [12–14],

✉ Jong-Hyun Lee
pljh@snut.ac.kr

[1] Department of Materials Science and Engineering, Seoul National University of Science and Technology, Seoul 01811, Republic of Korea

triethylene glycol [12, 15], diethylene glycol [12, 14, 16–18], CELTOL-IA [19], and ethylene glycol [20, 21] all decreased the decomposition temperature to between 110 and 160 ℃. This significant drop provided excellent sinter bonding between Ag finishes even at temperatures below 200 ℃ [19, 20]. However, to bond Cu finishes in air, their oxide layers should be eliminated and reoxidation at high temperature should be suppressed using an effective reducing agent in the paste [19]. Furthermore, the bonding temperature should be elevated to 300 ℃ to enhance the speed of sinter bonding under a specific compression [11], which may reduce the expected oxidation by the fast densification of the used particles in the bond line.

In a previous study on the sinter bonding of Cu finishes using Ag_2O paste at 300 ℃ under 5 MPa compression, a bonding time of 5 min was required after preheating for 10 min at 120 ℃, to attain a shear strength of approximately 29 MPa [12]. The interfacial bonding with the Cu finish was supported by a mixture of diethylene glycol and polyethylene glycol in the paste. Therefore, the intent of this study was to significantly shorten the bonding time under similar bonding conditions to a value acceptable for industrial application despite the use of low-cost Cu finishes. Furthermore, atomic-scale observation of the interface between the dissimilar metals (Ag and Cu) was performed to elucidate the principle of the interface bonding.

2 Experimental Procedure

2.1 Materials

The Ag_2O particles were synthesized by replacing the polyethylene glycol used in a previously reported method [22] with deionized (DI) water. The phase of the synthesized particles was confirmed by X-ray diffraction (XRD; DE/D8 Advance, Bruker). The Ag_2O particles were mixed with a commercial solvent (EW-10, Epsilon Epowder) that demonstrated excellent reducibility against copper oxide [23, 24] in a particle-to-solvent weight ratio of 7:3, using a spatula to prepare the paste.

2.2 Fabrication of Sintered Joints

The chip attachment was performed using a dummy chip (3×3 mm^2) and substrate (1 mm-thick Cu plate, 10×10 mm^2). The surfaces to be bonded were scrubbed using a 2000 mesh sandpaper and then etched in an ethanol-based 10% sulfuric acid solution. After printing the paste onto the substrate using a stencil mask with a $3 \times 3 \times 0.1$ mm^3 slit, the Cu chip was aligned onto the printed pattern. The sandwich-structured sample was transferred to a heating chuck, where it was rapidly heated to 300 ℃ in air at a rate of approximately 30 ℃/s while being simultaneously compressed with an external pressure of 2 or 5 MPa during the heating; the compression was then maintained at 300 ℃. The compression pressure was controlled by a pneumatic system at the first decimal place in the digital figure. Because the counting of the bonding time began immediately after the compression at the center region of a chip using a 14 mm-diameter collet, 30 s of bonding implied approximately 20 s at 300 ℃. The chip attachment process by high-speed sinter bonding and the heating profile are schematically shown in Fig. 1.

2.3 Characterization

The thermal behavior of the paste was examined using thermogravimetric and differential thermal analysis (TG–DTA; DTG-60, Shimadzu) during heating at a rate of 20 ℃/min. Furthermore, XRD (DE/D8 Advance, Bruker) and X-ray photoelectron spectroscopy (XPS, K-Alpha +, Thermo Fisher Scientific) analyses were conducted on the initial Ag_2O particles and particles that remained after heating the paste to 300 ℃ to characterize the chemical changes that occurred in the particles due to heating.

The bonding strength of the attached chip was evaluated by shearing using a micro-bond tester (Dage-4000, Nordson DAGE). The height of the shearing tip was 200 µm from the substrate surface, and the strength was defined as the maximum stress measured during shearing at 200 µm/s.

The morphology of the Ag_2O particles, cross-sectional microstructures of the formed bondlines, and fracture microstructures formed after the shear test were examined using high-resolution scanning electron microscopy (HR-SEM, SU8010, Hitachi). To distinguish the Ag and Cu phases in a micrograph, the microstructures were observed using the back-scattered electron (BSE) mode. The interface between the sintered Ag and bulk Cu was observed at an accelerating voltage of 200 kV using transmission electron microscopy (TEM; JEM-2010, JEOL).

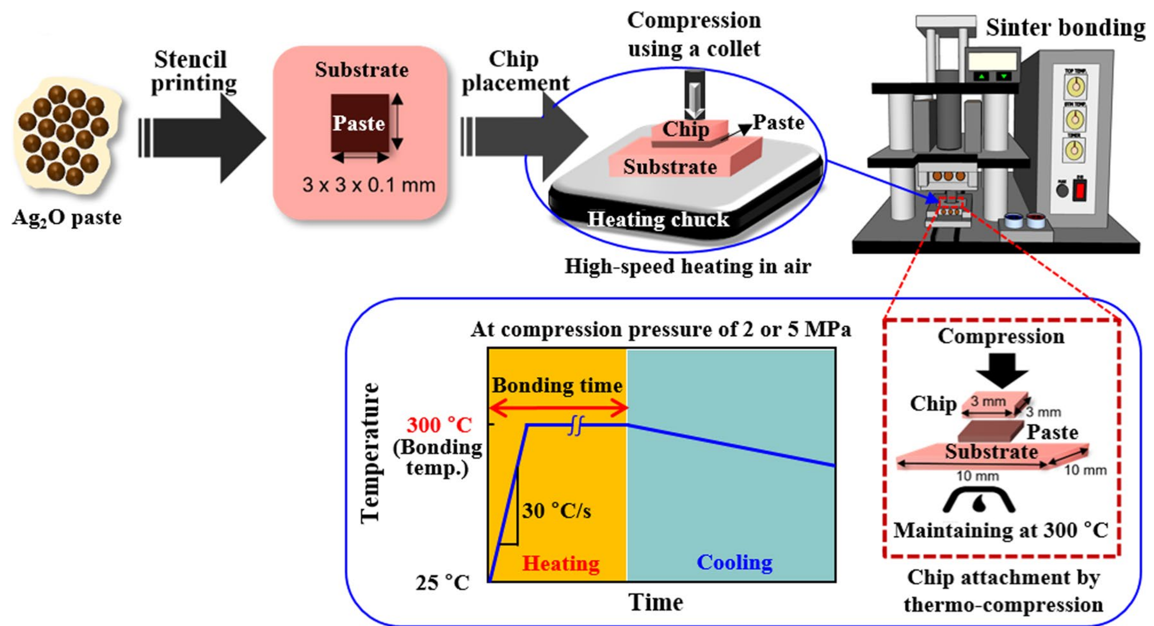

Fig. 1 Schematic diagrams depicting the chip attachment process by high-speed sinter bonding and the heating profile

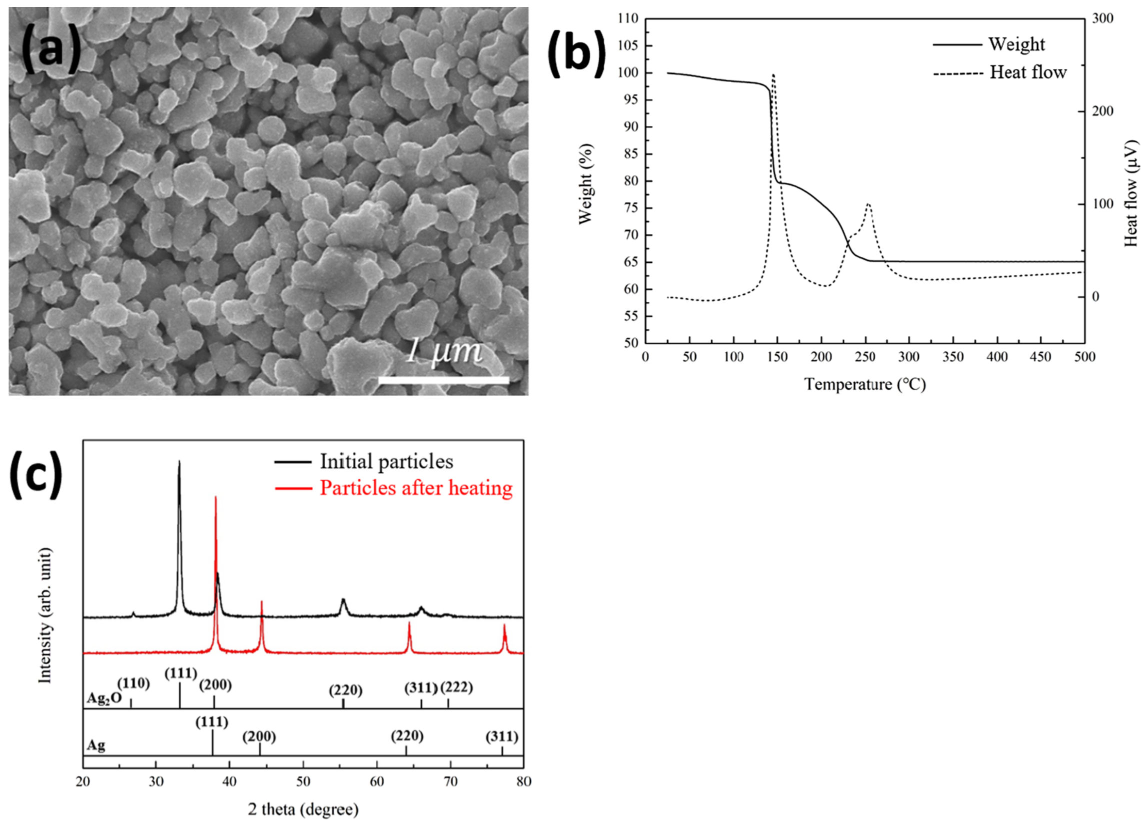

Fig. 2 **a** SEM image of synthesized Ag_2O particles, **b** TG–DTA results for prepared Ag_2O paste, and **c** XRD results for initial Ag_2O particles and particles remaining after heating to 300 ℃

3 Results and Discussion

3.1 Characteristics of Used Materials

The morphologies of the synthesized Ag_2O particles are shown in Fig. 2(a). Although the irregularly shaped particles were minuscule in size (161–253 nm), they did not undergo severe agglomeration. Particles in this size range can therefore be more suitable than nanoparticles for use as filler material owing to their low material cost, freedom from severe aggregation, and uniform dispersibility under simple planetary mixing.

Figure 2(b) shows the TG–DTA results for the prepared paste. Although Ag_2O particles normally undergo a decomposition reaction at approximately 400 ℃ that causes a decrease in mass [11] along with the formation of an endothermic peak, the paste containing both Ag_2O particles and the EW-10 solvent exhibited the start of a drastic loss of mass at 146 ℃ along with the formation of a large exothermic peak, as shown in Fig. 2(b). The exothermic peak formed due to the occurrence of a complex redox reaction in the paste [11–21], leading to the decomposition of Ag_2O and a consequent drastic decrease in mass of approximately 20 wt% at a temperature immediately below 150 ℃. Immediately after the reaction, the mass started decreasing at a completely different rate until the temperature reached 245 ℃ owing to the vaporization of the solvent, resulting in an additional loss of approximately 15 wt% of the paste. Lastly, another exothermic peak appeared in the temperature range of 210–295 ℃ with a peak temperature of 253 ℃, and the decrease in mass stopped with the formation of this peak. This peak was mainly attributed to the sintering behavior of the generated Ag. Based on the temperature at which the second exothermic reaction ended, 300 ℃ was concluded as a sufficiently high temperature for effective sinter bonding. Figure 2(c) shows the XRD analysis results of the particles remaining after the heating to 300 ℃ as well as the initial Ag_2O particles. The initial Ag_2O particles disappeared altogether after heating and only a pure Ag phase was observed, indicating that the heating caused reduction of Ag_2O into Ag.

Considering that Ag_2O decomposed at approximately 400 ℃ when exposed to air, the reaction of Ag_2O in the paste proceeding at a significantly low temperature can be attributed to its interaction with the solvent. The carbon and hydrogen atoms in the solvent surrounding the Ag_2O caused a thermodynamic reduction at the low temperature, which is explained by an Ellingham diagram [14, 25, 26]. When the Ag_2O reduced to Ag, the carbon and hydrogen atoms oxidized to form CO_2 and H_2O by combining with the released oxygen atoms and were then outgassed.

Figure 3 exhibits the XPS results for the Ag_2O particles before and after the redox reaction in the paste. For the initial Ag_2O particles before the reaction (Figs. 3(a) and 3(b)), two relatively broad peaks at binding energies of 368.18 and 374.18 eV are present in the Ag 3d spectra, while the Ag–O bond peak can also be observed at 529.58 eV in the O 1 s spectra [27], which indicate Ag^+ ions, confirming the existence of Ag_2O. Meanwhile, the XPS results for the particles remaining after heating the paste to 300 ℃ are shown in Figs. 3(c) and 3(d). The two peaks at 368.48 and 374.48 eV in the Ag 3d spectra are relatively sharp, and no Ag-related bond peak is present in the O 1 s spectra [27]. These results validate that Ag^0 metal remained after the decomposition of Ag_2O.

3.2 Sinter-Bonding Properties

Sinter bonding was conducted at 300 ℃ in air, and the shear strength values after the bonding with respect to the compression pressure and bonding time are shown in Fig. 4. When the pressure was 2 MPa, the significantly short bonding time of 30 s resulted in a sufficient shear strength of 27.8 MPa. The strength was much higher than that of a joint formed using a Pb-5Sn alloy, which is a representative high-melting-point solder [28]. Upon increasing the bonding time to 60 s, the strength increased to 37.4 MPa; however, this increase in the bonding time led to an eventual slight decrease in strength within the standard deviation range. Meanwhile, the 30 s bonding under 5 MPa presented a sufficient shear strength of 27.3 MPa, which consistently increased with increasing bonding time. Consequently, the 30 s results in Fig. 4 demonstrate never-before-reported fast sinter bonding between Cu finishes using a moderate pressure of 2 MP. The bonding time was only one-tenth that of previously reported results [12.13]. Moreover, it was found that at sufficient pressure (5 MPa), the shear strength increased with increasing in the bonding time.

3.3 Microstructures and Characteristics of Bondlines

The cross-sectional bondline structures after the 2 MPa bonding for different bonding times (30–300 s) are shown in Fig. 5. The bondline that formed after the short bonding time of 30 s exhibited a porous structure with many inter-particle

Fig. 3 XPS results for **a**, **b** initial Ag_2O particles and **c**, **d** particles remaining after heating the paste to 300 ℃: **a**, **c** Ag 3d spectra and **b**, **d** O 1 s spectra

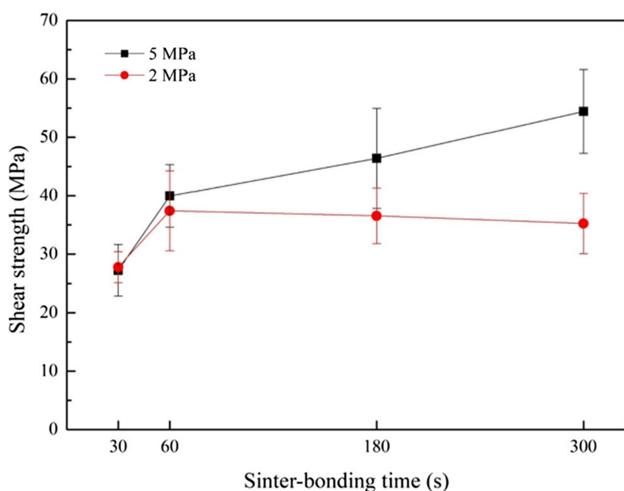

Fig. 4 Shear strengths measured after sinter bonding at 300 °C in air with different compression pressures and bonding times

voids. Nevertheless, the sintering between reduced Ag particles was sufficient, and the Ag particles were sintered to a similar degree with the upper and lower Cu finishes, which explained the sufficient strength obtained. The Ag atoms formed in situ by the redox reaction in the printed paste preferentially and rapidly generated Ag nanoparticles, which provided extraordinarily rapid sinterability during consistent thermo-compression for 30 s because of their active surface characteristics. Ag nanoparticles were also able to immediately sinter bond the Cu finishes after removing the surface oxide on the finish by the efficient reducing agent in paste. The samples that sinter-bonded for 60 s had a denser bondline structure. After 180 s and 300 s, the bondlines indicated the formation of Cu oxide layers at the upper and lower interfaces due to the penetration of oxygen through the porous bondline structure. Note that the upper and lower Cu oxide layers in the 180 s and 300 s bondlines were distinguished with a slightly different color from the

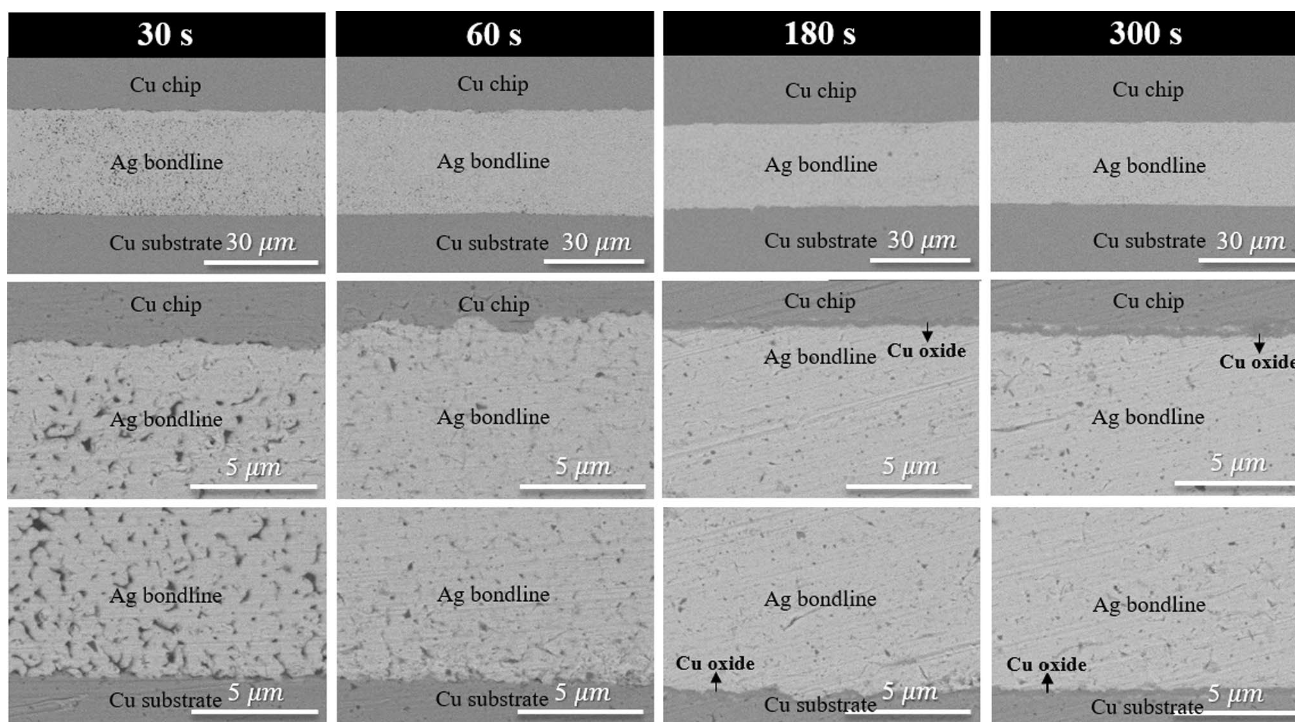

Fig. 5 Cross-sectional BSE images (whole and at the upper and lower interfaces) of bondlines after 2 MPa sinter bonding at 300 ℃ for different bonding times

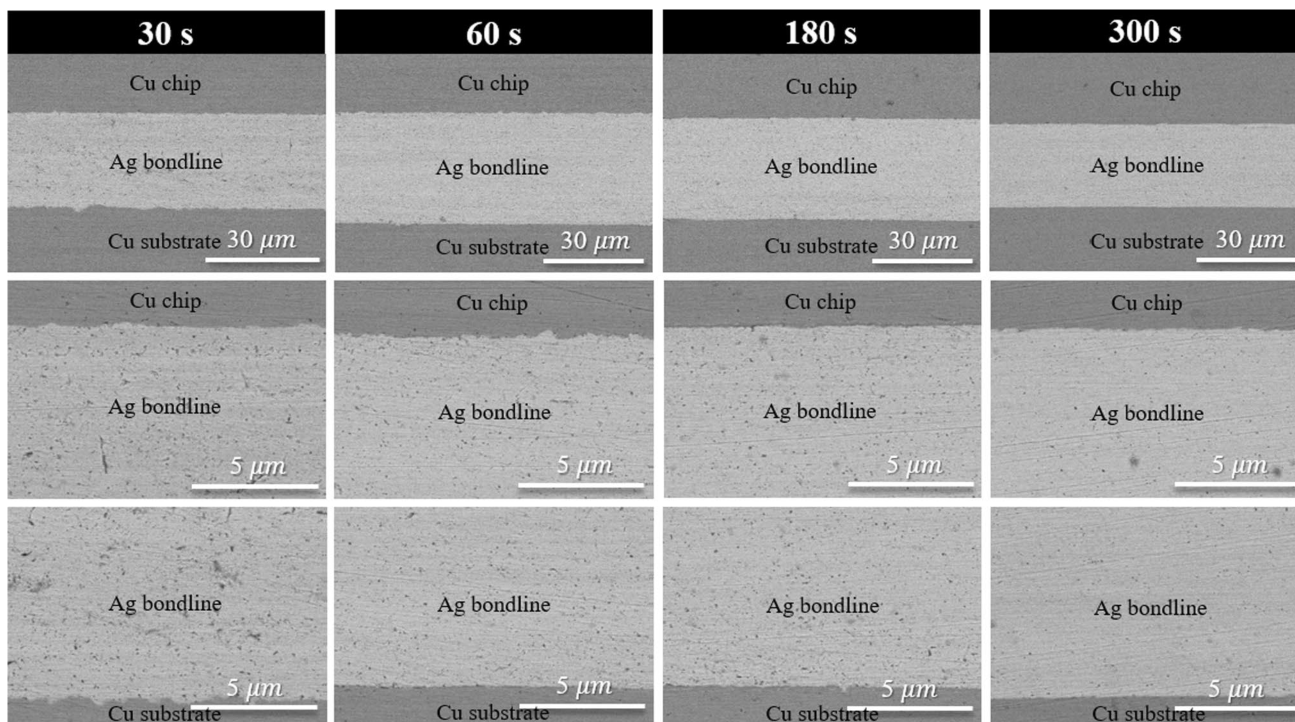

Fig. 6 Cross-sectional BSE images (whole and at the upper and lower interfaces) of bondlines after 5 MPa sinter bonding at 300 ℃ for different bonding times

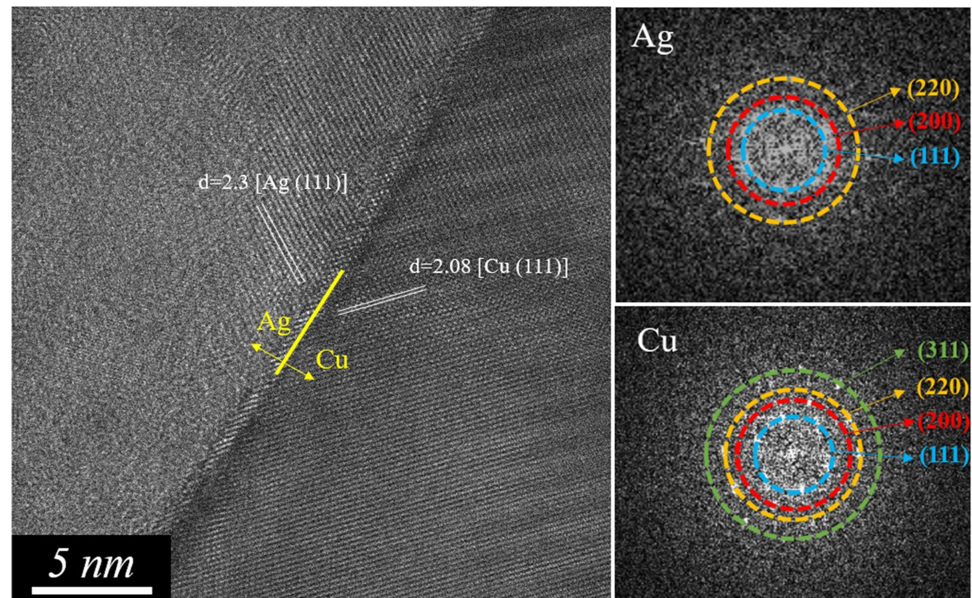

Fig. 7 High-resolution cross-sectional TEM image and FFT patterns at the Cu chip/Ag bondline interface after 5 MPa sinter bonding for 30 s

neighboring Cu. Energy dispersive spectroscopy (EDS) of the layer revealed that the oxygen amount exceeded 30 at%, confirming the formation of Cu_2O [6, 23, 29]. Moreover, the penetration of Ag into the Cu_2O/Cu interface increased with increasing bonding time [30]. The formation of oxide layers might have been involved in the decrease or stagnation in strength of the 2 MPa samples in Fig. 4.

Figure 6 shows cross-sectional BSE bondline images after the 5 MPa bonding for different bonding time. Compared to the structures observed in Fig. 5, the microstructural density and sintering degree in the bondline after the short bonding time of 30 s increased with the increase in compression pressure—a higher compression pressure accelerated the sintering between reduced nanoparticles and enhanced the bondline density after an identical bonding time. Thus, bonding for 60 s produced a near-full density in the bondline. Since then, the structure underwent an additional but minor improvement with a further increase in the bonding time.

More details about the microstructure of the Ag/Cu interface after 5 MPa bonding for 30 s are presented in Fig. 7. The fast Fourier transform (FFT) result for the Ag bondline region indicated the existence of (111), (200), and (220) planes. Tight bonding between the bidirectionally existing Ag and Cu at the interface was observed at the atomic scale. The large discrepancy between the Ag (111) and Cu (111) planes in the lattice parameter seemed to have been overcome by the inter-diffusion of Ag and Cu atoms. Moreover, layers with different lattice fringe spacings and directions were partially generated at the interface, which were analyzed to be Moiré fringes that were formed by the overlapping of the Ag and Cu lattices; furthermore, as observed from the Ag–Cu binary phase diagram, the formation of an intermetallic compound did not occur [31]. The microstructure implied that the Ag and Cu mutually diffused, with the inter-diffusion and lattice overlap acting as the bonding mechanisms between the Ag nanoparticles and Cu finish [29].

3.4 Fractography

Images of the fractures on the chip surfaces, formed by shearing after the 2 MPa bonding, are displayed in relation to the bonding time in Fig. 8. All the fractures occurred in patches at both the chip/bondline and bondline/substrate interfaces across the bondline. Therefore, the exposed Cu finish (dark gray color) in the chip/bondline interface (region 2) was observed in all the samples. The fracture pattern in the 60 s sample was more cluttered than that in the 30 s sample, which could have contributed to the enhanced bonding strength. However, the trend for the decrease or stagnation in strength for the 180 s bonding could be explained from the

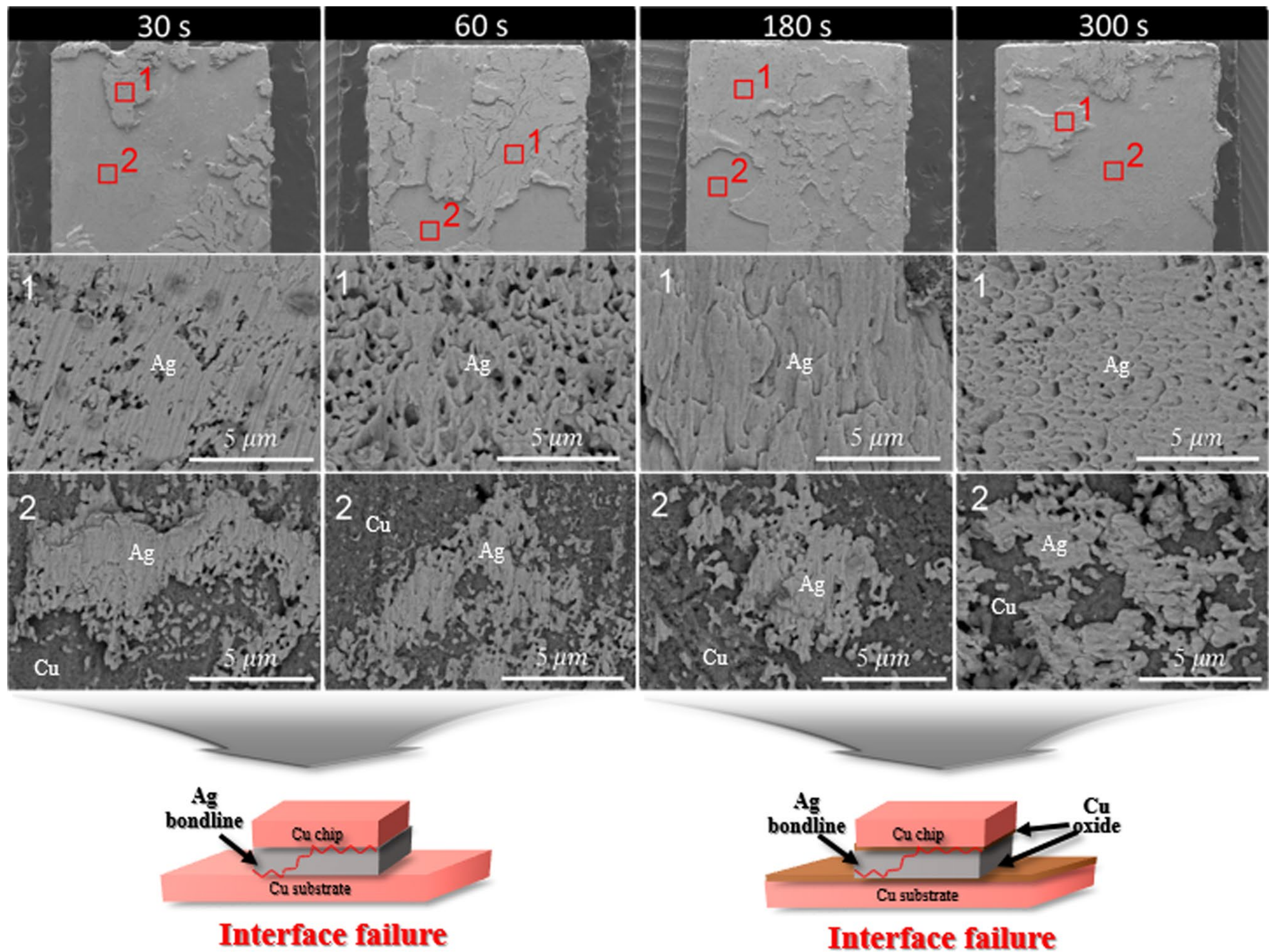

Fig. 8 BSE images of the fracture surface formed on a chip by the shear test after 2 MPa sinter bonding at 300 ℃ for different bonding times

results of Fig. 9. Figure 9(a) is a cross-sectional micrograph of the Cu chip/Ag bondline interface in a 180 s sample, and the formation of a Cu oxide layer at the interface can be seen in the micrograph. After confirming that the fracture mode after shear testing of the 180 s sample was that shown in the schematic of Fig. 9(b), the EDS result for the fracture surface was provided as Fig. 9(c). Consequently, the abnormally high oxygen content in the exposed Cu region implied the formation of a Cu oxide layer, and a failure in this layer lowered the shear strength by exhibiting brittle fracture behavior, depending on the degree of growth of the layer [12].

The fracture surfaces in the 5 MPa samples are exhibited in Fig. 10. Although the fracture modes were similar for all the bonding times tested, the size of the patch patterns reduced with increasing bonding time, making the fracture surface image cluttered. In addition, the sheared cup and cone fracture observed in a well-bonded metallic interface at the Ag fracture surface (region 1) elongated with increasing bonding time. The fracture trends agreed well with the measured strength results. The fracture surface at the chip/bondline interface (region 2) regularly included micro-regions of sintered Ag because of the higher compression.

4 Conclusions

To rapidly and cost-effectively achieve a bondline with long-term mechanical stability at high temperatures of 200–300 ℃ and excellent thermal conductivity, Ag_2O

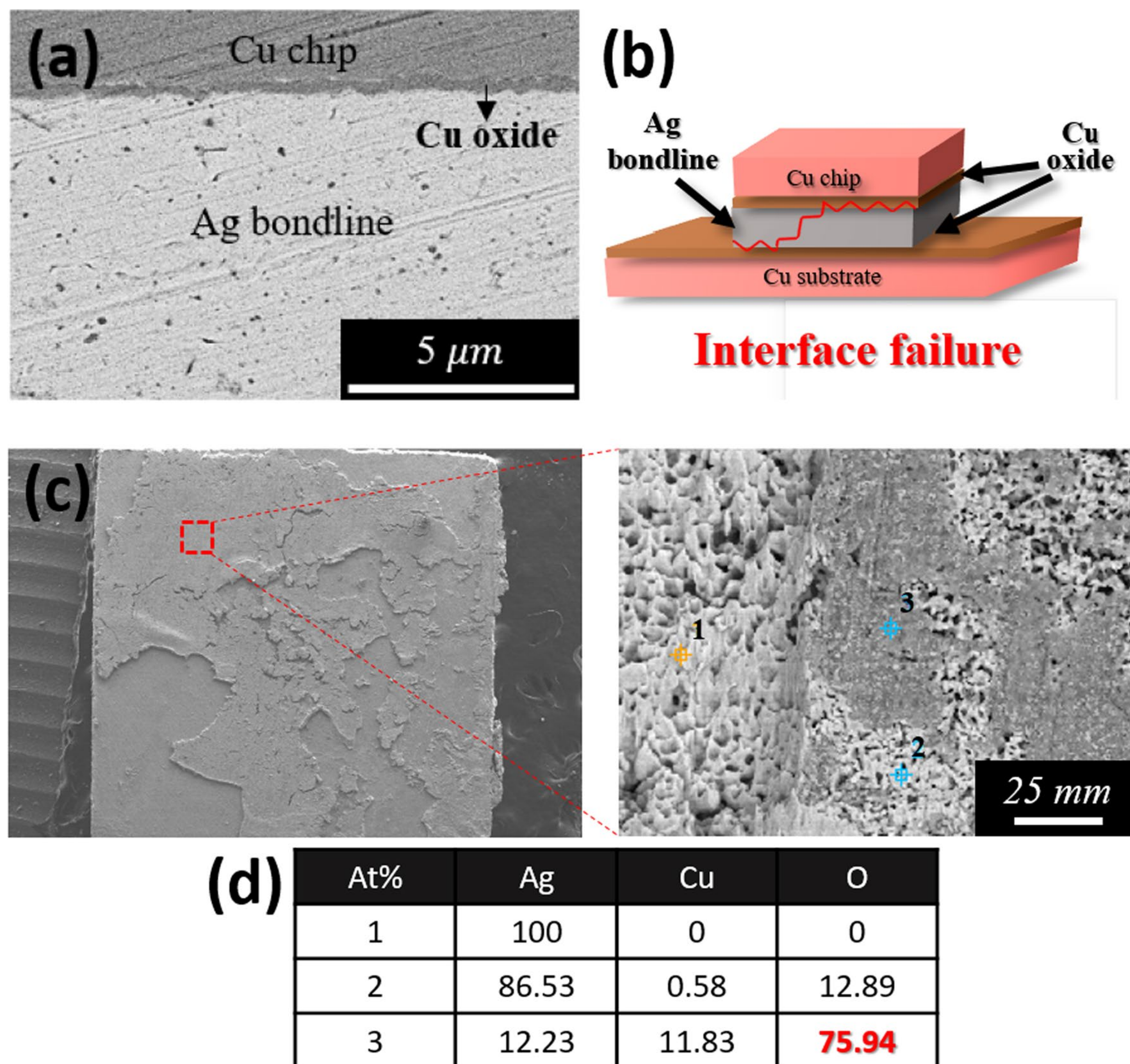

At%	Ag	Cu	O
1	100	0	0
2	86.53	0.58	12.89
3	12.23	11.83	75.94

Fig. 9 **a** Cross-sectional BSE image of Cu chip/Ag bondline interface in 180 s sample under 2 MPa and **b** schematic depicting fracture site in sample. **c** BSE image of the fracture surface formed on a chip in the 180 s sample and **d** EDS result at each region

particles sized ~ 200 nm were synthesized. Sinter bonding was performed between Cu finishes using a paste containing Ag_2O particles under moderate compression pressures of 2 and 5 MPa in an air atmosphere. Mixing the paste with the used reducing agent induced early decomposition of Ag_2O particles and the formation of an exothermic peak at 146 ℃, and the reduced Ag was rapidly sintered during the bonding at 300 ℃; XRD and XPS results confirmed the reduction of Ag by decomposition after heating to 300 ℃. Consequently, the paste provided a sufficient shear strength exceeding 27.0 MPa, inducing an effective and complete reduction of the Cu oxide even with after a significantly short bonding time of 30 s—the bonding time was only one-tenth that of previously reported results. The ultrafast bonding result was attributed to the radical sinterability of active Ag atoms generated in situ through a redox reaction in the paste under compression at 300 ℃. The obtained strength and dense bondline structure implied that this 30 s bonding method is appropriate for industrial production and applications.

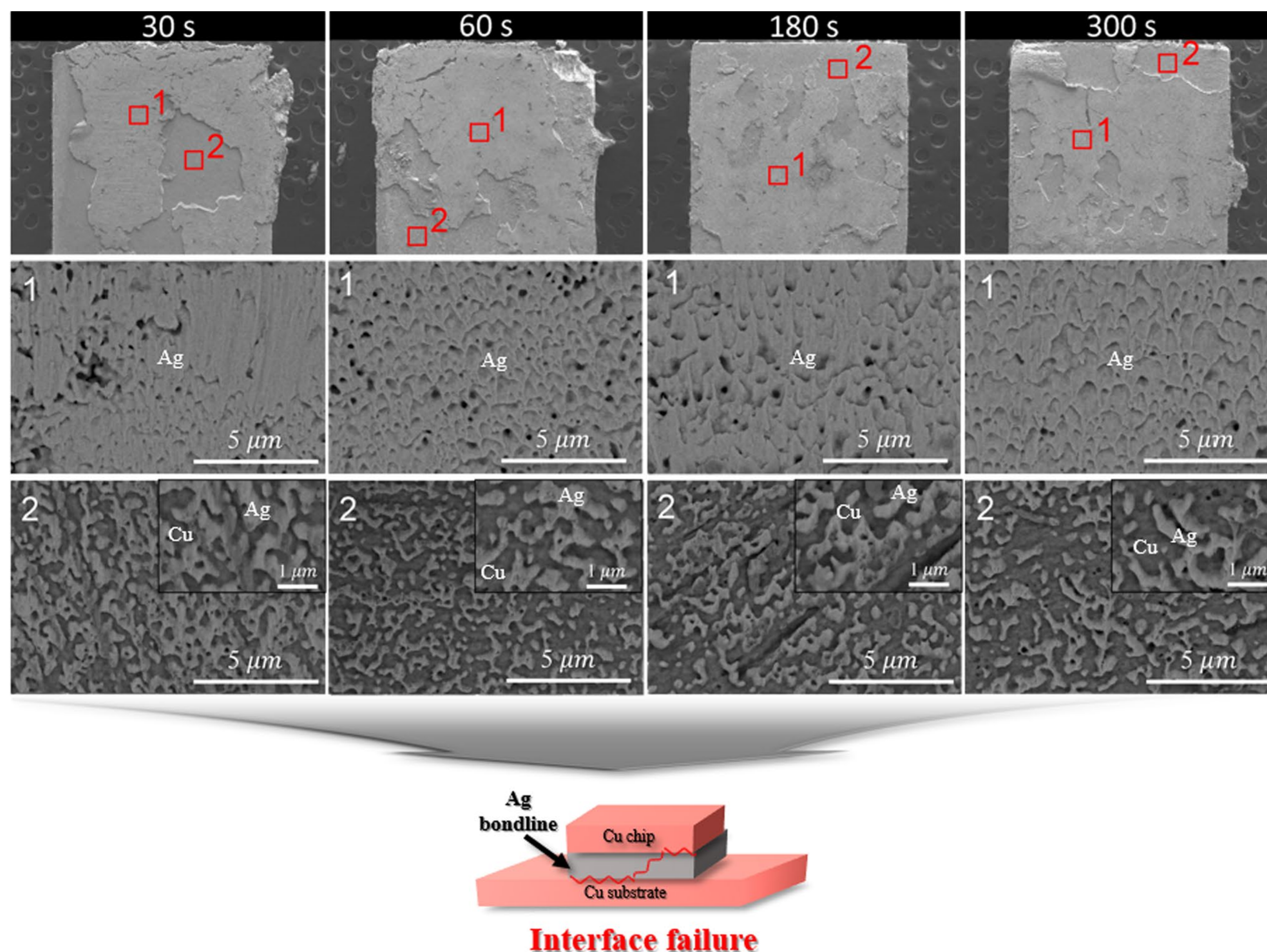

Fig. 10 BSE images of the fracture surface formed on a chip by the shear test after 5 MPa sinter bonding at 300 ℃ for different bonding times

Acknowledgements This work was supported by the National Research Foundation of Korea (NRF) grant funded by the Korea government (MSIT) (No: 2021R1A2C1007400). This paper was also supported by a Korea Institute for Advancement of Technology (KIAT) grant funded by the Korea Government (MOTIE) (P0008458, HRD Program for Industrial Innovation).

Declarations

Conflicts of interests The authors declare that they have no known competing financial interests or personal relationships that could have appeared to influence the work reported in this paper.

References

1. H.S. Chin, K.Y. Cheong, A.B. Ismail, Metall. Mater. Trans. B **41**, 824 (2010)
2. H. Zhang, C. Chen, J. Jiu, S. Nagao, K. Suganuma, J. Mater. Sci. Mater. Electron. **29**, 8854 (2018)
3. D. Kim, C. Chen, S. Noh, S.-J. Lee, Z. Zhang, Y. Kimoto, T. Sugahara. K. Suganuma, Microelectron. Reliab. **100–101**, 113380 (2019)
4. W.S. Hong, M.S. Kim, C. Oh, Y. Joo, Y. Kim, K.-K. Hong, JOM **72**, 889 (2020)
5. T.F. Chen, K.S. Siow, J. Alloys Compd. **866**, 158783 (2021)
6. S. Zhang, Q. Wang, T. Lin, P. Zhang, P. He, K.-W. Paik, J. Manuf. Process **62**, 546 (2021)
7. E.B. Choi, J.-H. Lee, Met. Mater. Int. **27**, 5278 (2021)
8. D. Namgoong, K.S. Siow, J.-H. Lee, Met. Mater. Int. (2022). https://doi.org/10.1007/s12540-022-01224-6
9. E. Ide, S. Angata, A. Hirose, K.F. Kobayashi, Acta Mater. **53**, 2385 (2005)
10. J. Yan, G. Zou, A. Wu, J. Ren, J. Yan, A. Hu, Y. Zhou, Scr. Mater. **66**, 582 (2012)
11. T. Morita, Y. Yasuda, E. Ide, Y. Akada, A. Hirose, Mater. Trans. **49**, 2875 (2008)
12. S. Takata, T. Ogura, E. Ide, T. Morita, A. Hirose, J. Electron. Mater. **42**, 507 (2013)
13. T. Ogura, T. Yagishita, S. Takata, T. Fujimoto, A. Hirose, Mater. Trans. **54**, 860 (2013)
14. T. Ogura, S. Takata, M. Takahashi, A. Hirose, Mater. Trans. **56**, 1030 (2015)
15. F. Mu, Z. Zhao, G. Zou, H. Bai, A. Wu, L. Liu, D. Zhang, Y.N. Zhou, Mater. Trans. **54**, 872 (2013)
16. T. Matsuda, K. Inami, K. Motoyama, T. Sano, A. Hirose, Sci. Rep. **8**, 10472 (2018)

17. K. Asama, T. Matsuda, T. Ogura, T. Sano, M. Takahashi, A. Hirose, Mater. Sci. Eng. A **702**, 398 (2017)
18. K. Motoyama, T. Matsuda, T. Sano, A. Hirose, J. Electron. Mater. **47**, 5780 (2018)
19. H. Zhang, Y. Gao, J. Jiu, K. Suganuma, J. Alloys Compd. **696**, 123 (2017)
20. L. He, J. Li, X. Wu, F. Mu, Y. Wang, Y. Lu, T. Suga, Metals **10**, 315 (2020)
21. Y.-J. Lee, J.-H. Lee, Electron. Mater. Lett. **18**, 94 (2022)
22. N.L. Yong, A. Ahmad, A.W. Mohammad, Int. J. Sci. Eng. Res. **4**, 155 (2013)
23. E.B. Choi, Y.-J. Lee, J.-H. Lee, J. Alloys Compd. **897**, 163223 (2022)
24. E.B. Choi, J.-H. Lee, Appl. Surf. Sci. **580**, 152347 (2022)
25. K.P. Jayadevan, N.V. Kumer, R.M. Mallya, K.T. Jacob, J. Mater. Sci. **35**, 2429 (2000)
26. I. Kim, S. Chun, J. Electron. Mater. **40**, 1977 (2011)
27. G.B. Hoflund, Z.F. Hazos, Phys. Rev. B **62**, 11126 (2000)
28. K. Suganuma, S.-J. Kim, K.-S. Kim, JOM **61**, 64 (2009)
29. S. Zhang, Q. Wang, T. Lin, P. Zhang, P. He, K.-W. Paik, J. Manuf. Process. **62**, 546 (2021)
30. J.H. Kim, J.-H. Lee, Jpn. J. Appl. Phys. **55**, 06JG01 (2016)
31. Y. Liu, S. Lin, H. Zhang, S. Nagao, C. Chen, K. Suganuma, Scr. Mater. **184**, 1 (2020)

Publisher's Note Springer Nature remains neutral with regard to jurisdictional claims in published maps and institutional affiliations.

Springer Nature or its licensor holds exclusive rights to this article under a publishing agreement with the author(s) or other rightsholder(s); author self-archiving of the accepted manuscript version of this article is solely governed by the terms of such publishing agreement and applicable law.